Soft Matter

Dynamic Article Links

Cite this: *Soft Matter*, 2012, **8**, 2956

www.rsc.org/softmatter

PAPER

Substrate and drying effect in shape and ordering of micelles inside CTAB–silica mesostructured films†

P. Chatterjee,[a] S. Hazra*[a] and H. Amenitsch[b]

Received 18th October 2011, Accepted 3rd January 2012
DOI: 10.1039/c2sm06982b

Deviation from a perfect 2D-hexagonal (*p*6*m*) structure, for CTAB–silica mesostructured films prepared by adding different amounts of excess ethanol to a solution of CTAB and TEOS just before spin coating on OH- and H-terminated Si substrates, is observed from combined X-ray reflectivity and grazing incidence small angle X-ray scattering measurements. Such a deviation can be well understood in terms of the shape and ordering of the micelles, with or without the silica coating layer's contribution, inside the film. For example, cylindrical shaped micelles, which are initially circular on a hydrophilic OH-terminated Si substrate in order to form a perfect 2D-hexagonal structure, become elliptical (extended along the in-plane) on a hydrophobic H-terminated Si substrate to form a slightly compressed 2D-hexagonal structure due to a different attachment of the film to the substrate. With time, due to the drying of the silica materials and its restricted movement along the in-plane direction, the films on both the substrates are compressed along the out-of-plane direction only, to form observed centered rectangular (*c*2*mm*) structures. Also, due to the asymmetric shrinkage, stress is developed, which deteriorates the ordering in the film. The final shape of the micelles, including the silica coating layer's contribution, shows maximum and minimum deviations from the circular shape inside the thick film on a OH–Si substrate and the thin film on a H–Si substrate, respectively. The deviation in the shape of the micelles itself, which is of actual importance, seems to be maximum and minimum inside the thick film on a H–Si substrate and the thin film on a OH–Si substrate, respectively, and is essentially determined by the substrate nature and initial silica wall thickness.

1. Introduction

Surfactant-templated mesostructured silica materials, discovered by Mobil researchers in 1992,[1] are the subject of intense research due to their potential applications as membranes, low dielectric constant insulators (so-called low κ-materials), sensors and optoelectronic devices *etc.*[2–5] In many applications, such materials are often required to be in the form of thin films, which can be grown by a procedure called evaporation-induced self-assembly (EISA).[2] The process begins with a homogeneous solution of surfactant, soluble silica, alcohol and water in acidic conditions to minimize the siloxane condensation. The concentration of surfactant in the solution is kept above the critical micelle concentration (cmc) to form aggregates (called micelles) of different shapes such as, spheres, cylinders and layers *etc.* During film deposition by dip-coating or spin-coating, self-assembly and further organization of micelles takes place by evaporation of the solvent, which produces lamellar, two-dimensional (2D) hexagonal (*p*6*m*), three-dimensional (3D) hexagonal ($P6_3$–*mmc*), or cubic (*Pm*3*n*) mesostructures.[6–9] The structures of the micelles depends on the solution conditions and in many cases can be rationalized by considering intermolecular forces.[10,11] Apart from the surfactant : silica ratio, other parameters like the aging of the initial silica sol after the hydrolysis, relative humidity of the environment, nature of the silicon alkoxide and temperature of the solution *etc.* are important to control the nature of the silica mesophase and the quality of the organization in films.[12–14]

The normal self-assembly process of the surfactant molecules at an interface can be different from that in the bulk solution because it is perturbed by competing surfactant–surface and solvent–surface interactions, which can lead to different structures. The adsorption of surfactant molecules on solid surfaces in aqueous solutions has attracted much attention in the field of colloid and surface chemistry because of its interesting physical and chemical properties. Recently, adsorbed surfactants at different solid–liquid interfaces have been widely studied mainly using atomic force microscopy to obtain direct images of surface aggregates at the interface between solid substrates and aqueous solutions.[15–21] These studies suggest the strong role of substrate

[a]*Surface Physics Division, Saha Institute of Nuclear Physics, 1/AF Bidhannagar, Kolkata, 700064, India. E-mail: satyajit.hazra@saha.ac.in*
[b]*Institute of Biophysics and Nanosystem Research, Austrian Academy of Sciences, Schmiedlstrasse 6, 8042 Graz, Austria*

† Electronic supplementary information (ESI) available. See DOI: 10.1039/c2sm06982b

This journal is © The Royal Society of Chemistry 2012

surface conditions, apart from concentration of the surfactant, in structure formation through different attachments. The substrate surface condition can be modified through termination of the surface with an OH or H group, which essentially modifies the surface free energy, polar–nonpolar (hydrophilic–hydrophobic) or electrostatic nature of the surface.[22–28] However, not much systematic work has been carried out to understand the role of such substrate surface conditions on the initial attachment of silica coated surfactant molecules, which can not only control the initial mesostructure of the film,[29] but also the final mesostructure through subsequent drying. Moreover, understanding the role of alcohol on those structures and their control is very important, as it is known that alcohol can act as a cosolvent or cosurfactant and can modify the mesostructure accordingly.[9,30]

In order to understand these issues, mesostructured films (by selecting fixed ratio of surfactant and silica) were prepared after adding different amounts of excess alcohol before spin coating on OH- and H-terminated Si substrates and they were then characterized using complementary X-ray reflectivity (XR)[25,26,28,31,32] and grazing incidence small angle X-ray scattering (GISAXS)[8,33–38] techniques. Formation of compressed 2D-hexagonal or centered rectangular (*c2mm*) mesostructures (as shown schematically in Fig. 1) with disorder by deviating from a perfect 2D-hexagonal structure (for which $d_{11} = d_{02}$, $r_l = r_s$ and $c/b = \sqrt{3}$), are observed. The possible role of substrate surface, excess alcohol and drying on such structural deformation, are discussed.

2. Experiment

2.1 Preparation

A silica–surfactant solution was prepared using tetraethyl orthosilicate [TEOS, $Si(OC_2H_5)_4$, Sigma Aldrich, 99.999%] as the silica source, cetyltrimethylammonium bromide [CTAB, $C_{16}H_{33}N(CH_3)_3Br$, Fluka, ≥99%] as the structure directing surfactant agent, ethanol [C_2H_5OH, Merck, absolute] and Milli-Q water (resistivity 18.2 MΩ cm^{-1}) as the common solvent and hydrochloric acid [HCl, Merck, 35%] as the catalyst. The precursor solution was prepared in two steps. In the first step, a silica solution was prepared by hydrolysis and condensation of TEOS in acidic conditions. For this step, the silica solution was prepared in the molar ratio of TEOS : C_2H_5OH : H_2O ≈ 1 : 4.5 : 1 and finally the required amount of HCl was added to the solution to keep the pH ≈ 1. The solution was then stirred for 1 h at room temperature. In parallel, a second solution was prepared by dissolving CTAB in ethanol and water (in the molar ratio of CTAB : C_2H_5OH : H_2O ≈ 1 : 82 : 24). In the second step, the second solution was added to the first one to get the final solution in the molar ratio of TEOS : CTAB : C_2H_5OH : H_2O = 1 : 0.19 : 20 : 5.5, which was then stirred for another 1 h and aged for 2 h. Different diluted solutions were then prepared by adding excess ethanol (of amount $\phi = 15$, 20, 30 and 35 cm^3) to the stock solution (of amount about 9 cm^3) to see the effect of alcohol on the mesostructure.

Hydrophilic and hydrophobic Si(001) substrates (of size 15 × 15 mm^2) were prepared through different pre-treatment, as reported before.[28] In short, one set of substrates was treated with the RCA cleaning method, where the substrates were boiled at 100 °C for about 15 min in a mixed solution of ammonium hydroxide [NH_4OH, Merck, 30%], hydrogen peroxide [H_2O_2, Merck, 30%] and Milli-Q water (NH_4OH : H_2O_2 : H_2O = 1 : 1: 5, by volume). The substrates were then rinsed thoroughly with Milli-Q water. A fresh oxide layer, which is terminated with an OH group, was grown on the Si surface after removing the native oxide layer by such a treatment. The OH-terminated Si substrate (labeled as OH–Si) is hydrophilic in nature. Another set of substrates was etched with a solution of hydrogen fluoride [HF, Merck, 10%] for about 30 s at room temperature (25 °C) to passivate the Si surface with H after removing the native oxide layer. Such a H-terminated Si substrate (labeled as H–Si) is hydrophobic in nature.

Films were then prepared (at temperature: 25–30 °C and relative humidity: 70–75%) using a spin-coater (EC101, Headway Research) at a speed of 4000 rpm. The films prepared from differently diluted (stock and 15, 20, 30 and 35 cm^3 excess ethanol added) solutions on hydrophilic OH–Si substrates, are labeled as OH(0), OH(15), OH(20), OH(30) and OH(35), and on hydrophobic H–Si substrates (within 5 min after treatment), are labeled as H(0), H(15), H(20), H(30) and H(35). Samples were then preserved at the X-ray laboratory, where temperature and relative humidity were maintained at ∼25 °C and ∼40%, respectively.

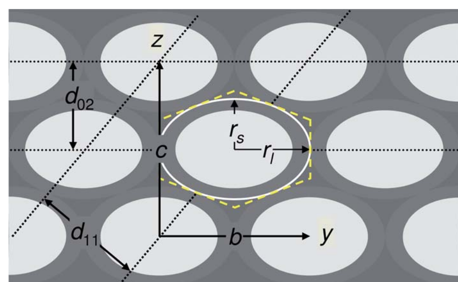

Fig. 1 Schematic of the compressed 2D-hexagonal *i.e.* centered rectangular (*c2mm*) mesostructure with unit cell parameters (*b* and *c*), lattice spacings (d_{02} and d_{11}), the Wigner–Seitz cell (yellow dashed lines) and corresponding ellipse (white curve) with semi-major (r_l) and semi-minor (r_s) axis.

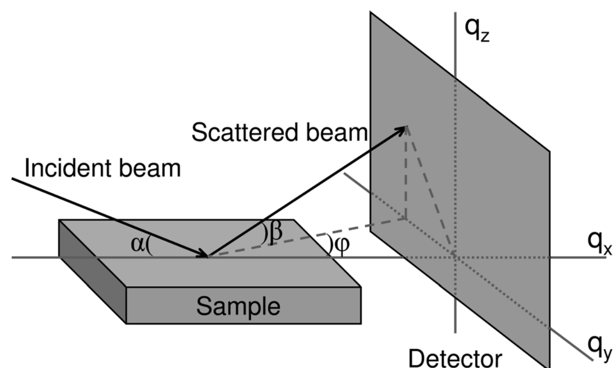

Fig. 2 Schematic of the scattering geometry used to perform X-ray measurements.

2.2 Characterization

The scattering geometry used for the characterization of samples is shown schematically in Fig. 2. The surface of the sample is in the x–y plane and the incident X-ray beam (of wavelength λ) is in the x–z plane. α is the incident angle with the x–y plane and β and φ are the exit angles with the x–y and x–z planes, respectively. In this reflection geometry, the components of the wave vector transfer, $\vec{q}\,(\boldsymbol{q}_x, \boldsymbol{q}_y, \boldsymbol{q}_z)$, are $\boldsymbol{q}_x = (2\pi/\lambda)(\cos\beta\cos\varphi - \cos\alpha)$, $\boldsymbol{q}_y = (2\pi/\lambda)(\cos\beta\sin\varphi)$ and $\boldsymbol{q}_z = (2\pi/\lambda)(\sin\beta + \sin\alpha)$.

XR measurements were performed on a versatile X-ray diffractometer (VXRD) setup[39] as a function of time (the first measurement of each sample was carried out after 15 h from preparation) to see the effect of drying on the structure of the film. VXRD consists of a diffractometer (D8 Discover, Bruker AXS) with Cu source (sealed tube) followed by a Göbel mirror to select and enhance Cu–Kα radiation (λ = 1.54 Å). The diffractometer has a two-circle goniometer [$\theta(\omega) - 2\theta$] with a quarter-circle Eulerian cradle as the sample stage. The latter has two circular (χ and ϕ) and three translational (X, Y, and Z) motions. The scattered beam was detected using a NaI scintillation (point) detector. Data were taken in the specular condition, *i.e.* for $\varphi = 0$ and $\alpha = \beta = \theta$. Under such conditions there exists a nonvanishing wave vector component, $\boldsymbol{q}_z$, which is equal to $(4\pi/\lambda)\sin\theta$ with a resolution of 0.003 Å^{-1}. On the other hand, GISAXS measurements of the dried films were performed using a synchrotron source (SAXS beam line, Elettra) at energy 8 keV.[40] The scattered beam was detected using a 30 cm diameter (2000 × 2000 pixel) image plate detector (mar300, Marresearch GmbH), by placing it about 90 cm apart from the sample. For data collection, α was kept (0.5–0.6°) slightly greater than the critical angle, α_c, of the sample. The direct beam was stopped and the specular reflected beam was attenuated to avoid the saturation of the detector.

It is known that XR provides an electron-density profile (EDP), *i.e.*, in-plane (x–y) average electron density (ρ) as a function of depth (z) in high resolution,[25] from which one can estimate the total film thickness (t), the average porosity, the film–substrate interface and the value of d_{02} (or c), while GISAXS provides both out-of-plane and in-plane structures[8,38] *i.e.*, the value of d_{02} and d_{11}, from which one can extract the value of c and b, related to the centered rectangular unit cell parameters and also r_s and r_l, related to the ellipse of the corresponding Wigner–Seitz cell (see Fig. 1). The ratio of r_l and r_s can provide the information about the deviation from perfect 2D-hexagonal structure.

3. Results and discussion

3.1 XR: Interface and out-of-plane structures

XR data of OH(0) and H(0) CTAB–silica films measured initially (after 15 h) and finally (after 2 months) are shown in Fig. 3. The presence of a pseudo Bragg peak (around $\boldsymbol{q}_z$ = 0.2 Å^{-1}) with a slightly varying position (see insets of Fig. 3) is evident in each curve. Also, the nature of the reflectivity profile (or fall of intensity), after the Bragg peak, is not the same. For the OH(0) film, the fall is sharp followed by a small dip, while for the H(0) film, the fall is more gradual. The absence of any Kiessig fringes in the curves indicates that the films are quite thick, while the presence of a pseudo Bragg peak indicates the existence of a repeating layer structure in the film. Such repeating layers arise from the periodic arrangement of the cylindrical micelles in the polymeric silica matrix to form a 2D-hexagonal structure, which corresponds to the (02) Bragg peak of the equivalent rectangular unit cell (see Fig. 1). The second order Bragg peaks, which are present in the initially-measured films, are almost absent in the finally-measured or dried films. Also, the intensity of the first Bragg peak decreases considerably for the dried films, which indicates that the ordering in the structure of the films deteriorates with time. Values of d (*i.e.* d_{02}), obtained from the (02) Bragg peaks, are tabulated in Table 1. The decrease in the values

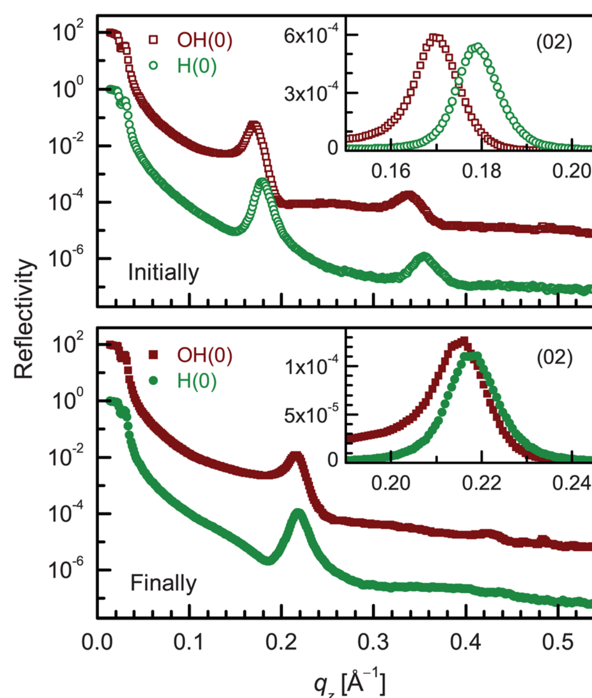

Fig. 3 XR data of CTAB–silica mesostructured thick films on differently-terminated Si substrates, measured initially (after 15 h) and finally (after 2 months) (curves are shifted vertically for clarity). Insets: magnified view of corresponding first order (02) Bragg peak to have a better idea about their position and intensity.

Table 1 Parameters, such as the separation (d) corresponding to the first order (02) Bragg peaks and its shrinkage (Δd) with time, the total film thickness (D) and the number of repetitive layers (N) for the films on differently-terminated Si substrates as obtained from XR data. Subscripts i and f represent parameters corresponding to the initial and final time of measurements, respectively

Sample	d_i (nm)	d_f (nm)	Δd (nm)	D_i (nm)	D_f (nm)	N
OH(0)	3.71	2.91	0.80			
H(0)	3.52	2.89	0.63			
OH(15)		3.04			55	17
H(15)		3.20			58	17
OH(20)		3.13			49	15
H(20)		3.19			55	16
OH(30)		3.13			39	11
H(30)		3.19			41	11
OH(35)	3.82	3.16	0.66	38	33	9
H(35)	3.74	3.40	0.34	38	35	9

 This journal is © The Royal Society of Chemistry 2012

of d with time is clearly evident, which is related to the drying. However, such a decrease is different for films on differently-terminated substrates and is more for the OH(0) sample, where the initial value of d was large. This suggests that although a 2D-hexagonal structure is formed on both terminated surfaces, the size, shape or separation of the micelles is probably not the same. To predict further from the XR data, extraction of EDP is necessary, which is possible for thin films, as discussed next.

XR data of OH(35) and H(35) CTAB–silica films measured initially (after 15 h) and finally (after 2 months) are shown in Fig. 4. Unlike thick films, Kiessig fringes are present in the curves indicating the low thickness of the films. Well resolved first and second order (02) Bragg peaks are observed in all the curves. The intensity of both the peaks decreases for the dried films. This indicates that the ordering in the structure of such thin films deteriorates with time, however, the ordering is better compared to the thick films. The values of d, obtained from the (02) Bragg peak positions, are tabulated in Table 1. It is clear from the table that for the thin films the value of d decreases with time and such a decrease is less for the film on the H–Si substrate, similar to that observed for the thick films. However, the values of d obtained for the thin films are more compared to those of the thick films and the change in the values of d, due to drying, for both the thin films is much less compared to that for the thick films.

To get further information about the thin films, EDPs have been extracted by analyzing the XR profiles using Parratt's formalism.[41] For the analysis, a model of oscillatory electron density profile, arising from periodic repetitions of two stacked layers with roughness at each interface, is considered. One layer is made of cylindrical surfactant aggregates plus a silica wall, having an averaged electron density ρ_1, a thickness t_1 and a roughness σ_1. Another layer is made of silica only, with an electron density ρ_2, a thickness t_2 and a roughness σ_2. Depending upon the substrate nature the initial attachment may be different, which is also considered in the model. The best fit XR profiles of the films on two differently-terminated substrates along with the corresponding EDPs thus obtained are shown in Fig. 4.

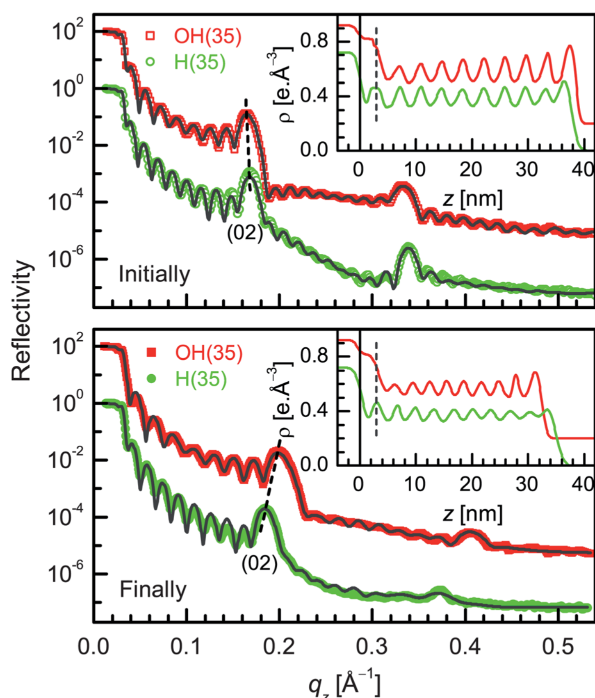

Fig. 4 XR data (different symbols) and analyzed curves (solid line) of CTAB–silica mesostructured thin films on differently-terminated Si substrates, measured initially (after 15 h) and finally (after 2 months) (curves are shifted vertically for clarity). The position and movement of the first order (02) Bragg peak are indicated by the dashed line. Insets: corresponding EDPs, showing possible structures of the films on different surfaces with different film–substrate layers (between solid and dashed straight lines).

The EDPs near the film–substrate interface for two films are quite different. For the OH(35) film, after the substrate there is an intermediate plateau region followed by a dip, while for the H(35) film a sharp dip after the substrate is evident. The width of the dip is again different. The plateau and dip regions correspond to silica and micellar layers, respectively. Such a silica layer is arising partially from the oxidation of Si substrate after RCA treatment and partially from the coating of micelles. The absence of a silica layer on the H–Si substrate indicates direct attachment of micelles on it. Such attachment is *via* a hemicylindrical micellar layer as the small width of the dip suggests. It is necessary to mention that the different nature in the fall of intensity after the Bragg peaks on differently-terminated substrates is related to these different types of attachment.

The EDPs (Fig. 4) show that after the initial film–substrate layer (of thickness d_{fs}), both the films consist of N number of repetitive cylindrical micellar layers, where the top silica layer has extra thickness (d_t). The repetitive layers are uniformly spaced throughout the film with an average separation d. The values of N and the total film thickness ($D = d_{fs} + N \times d + d_t$) are enlisted in Table 1 along with the values of d. For the films measured initially, the value of d on the OH–Si substrate is larger than that on the H–Si substrate, which may be related to the shape of the micelles. It is expected that due to the different attachment of the film with the substrate, the spherical shape of micelles on a hydrophilic substrate may become elliptical (with large in-plane size and small out-of-plane size) on a hydrophobic substrate. Furthermore, it is observed from the EDPs that the ordering of micelles on the H–Si substrate is nearly uniform, while on the OH–Si substrate, it is better towards the top. With time the separation decreases and the ordering deteriorates for both the films. The deterioration in the ordering with time is likely to be related to the stress developed due to asymmetric shrinkage of the film, namely shrinkage only allowed along the z-axis but not in the x–y plane. The decrease in separation, which is mainly related to the drying of the silica materials, not only decreases the silica wall thickness but also the size of the micelles along out-of-plane direction, as is evident from the EDPs. The decrease is however more on the OH–Si substrate, suggesting a definite role of the initial shape of the micelles. The asymmetric shrinkage, which tries to make the shape of the micelles elliptical (by compressing along out-of-plane direction), is likely to have more of an effect if the initial shape is spherical rather than elliptical. The value of N is found to be same (9) for both the films. However, the value of D for both the samples, which was similar at the time of initial measurements, finally becomes different due to the different change in the value of d with time.

In order to understand any systematic influence of excess alcohol on the structure of the films on both the substrates, XR curves for the dried films of different alcohol content (thus of different thickness) on hydrophilic (OH–Si) and hydrophobic (H–Si) substrates are shown in Fig. 5 and Fig. 6, respectively. The shift of the (02) Bragg peak towards the lower $\boldsymbol{q}_z$ value with an increase of excess ethanol in the solution is observed. The value of d_f obtained from the peak position and the value of D_f obtained from the Kiessig fringes (for the films grown on OH–Si substrates, initial silica layer thickness was also included) are listed in Table 1, which indicate the increase in the value of d_f and the decrease in the value of D_f with the increase of excess alcohol in the solution. From the value of D_f it is possible to find out the value of N, which is also listed in Table 1. The addition of alcohol in the solution just before deposition is to dilute the solution, hence to decrease the viscosity, which is observed in the value of D_f, but not in the value of d_f. The increase in the value of d_f, which is related to the micelle size and the silica coating thickness, apparently suggests that the increase in the micelle size is large compared to the decrease of the silica wall thickness.

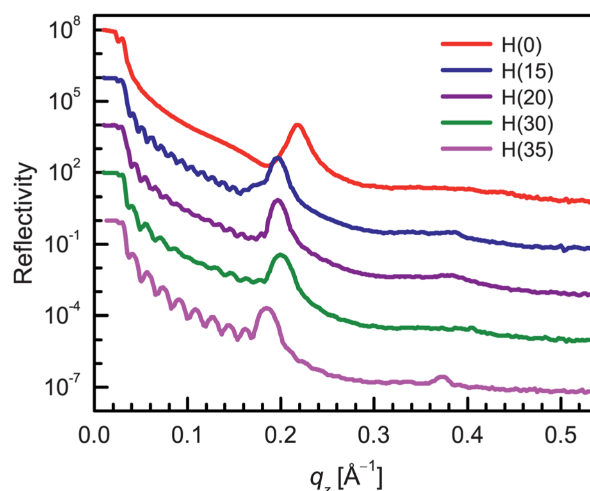

Fig. 6 XR data of CTAB templated mesostructured dried silica films of different thickness deposited on H-terminated hydrophobic Si substrates. Curves are shifted vertically for clarity.

3.2 GISAXS: In-plane and out-of-plane structures

So far, we have discussed XR results, which essentially provide the information about the out-of-plane separation between the micelles in the films and the attachments of the films with the substrates. Such information allows us to predict possible structures of the films and the role of different parameters, such as the hydrophobic–hydrophilic nature of substrate, the cosolvent–cosurfactant nature of alcohol or the stress effect of drying, on the structure formation. However, to ascertain the prediction, structural information along both (out-of-plane and in-plane) directions, which can be obtained from GISAXS results, is very important and will be discussed now. GISAXS patterns of the dried CTAB–silica mesostructured films of different thickness on differently-terminated Si substrates are shown in Fig. 7. (02) and (11) Bragg spots, signatures of a compressed 2D-hexagonal structure, are evident in all the patterns. In-plane (b) and out-of-

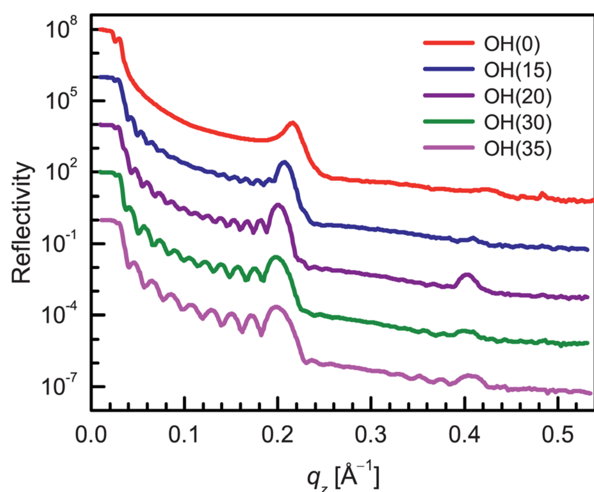

Fig. 5 XR data of CTAB templated mesostructured dried silica films of different thickness deposited on OH-terminated hydrophilic Si substrates. Curves are shifted vertically for clarity.

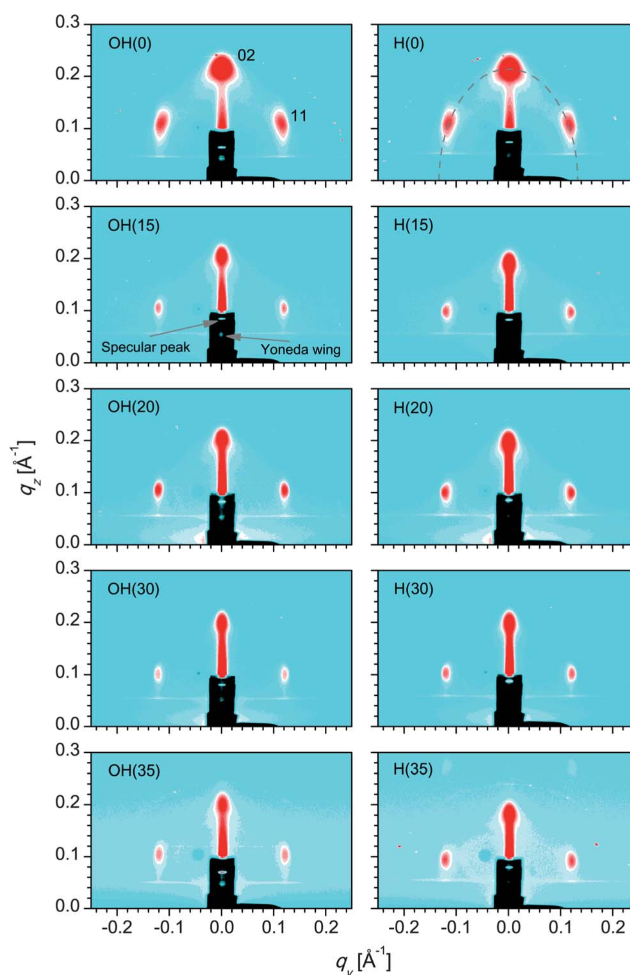

Fig. 7 GISAXS pattern of the CTAB templated dried silica films of different thickness on hydrophilic and hydrophobic Si substrates, showing (11) and (02) peaks of the compressed 2D-hexagonal structure, semi-elliptical ring (dashed line) used for the estimation of the ratio (r_l/r_s) and also the specular peak and Yoneda wing (indicated by arrows).

This journal is © The Royal Society of Chemistry 2012

plane (c_f) structural parameters for all the dried films, extracted from GISAXS spots are listed in Table 2 and plotted as a function of excess alcohol (ϕ) in Fig. 8(a). It is necessary to mention that the value of c_f obtained from the GISAXS measurements is consistent with that of c_f (= $2d_f$) obtained from the XR measurements (Table 1). A specular peak and Yoneda wing are also observed in the GISAXS patterns, which correspond to the incident angle (α) and the critical angle (α_c), respectively.

Fig. 8(a) shows that the value of b decreases (however small), unlike c_f, with excess-alcohol content. This is in contradiction with the prediction that the increase in the size of micelles is larger than the decrease in the silica coating thickness. To understand the actual situation, we have investigated the ratio of semi-major and semi-minor axis (r_l/r_s) of the ellipse,[42] as defined in Fig. 1. The values of $(r_l/r_s)_f$, estimated from $\sqrt{3}/(c_f/b)$, are listed in Table 2. These values agree well with the values estimated from the semi-elliptical ring[42] as indicated in Fig. 7. The variation of $(r_l/r_s)_f$ with ϕ is shown in Fig. 8(b). Also, to understand the effect of drying, the value of c_i (= $2d_i$) for the thick and thin films obtained from the initial XR measurements and the corresponding ratio $(r_l/r_s)_i$, considering b remains unchanged with time, are listed in Table 2 and also included in Fig. 8. It is clear from Fig. 8 that the shape of the silica layer coated micelles in the films changes with the addition of excess alcohol in the solution, even in the initial stages of measurements. However, the change ($\sim$0.1) is small compared to the dried films (>0.2). With time the change in the value of r_l/r_s for the films on OH–Si is more compared to that on H–Si. Correspondingly, the value of $(r_l/r_s)_i$ for the films on H–Si is slightly larger than that on OH–Si, while the value of $(r_l/r_s)_f$ are reversed.

The variation of different parameters, plotted in Fig. 8, can be expressed quantitatively using standard exponential dependence. First consider the size ($2R$) of circular micelles. Presuming no drastic change in the shape of the micelles in our experimental alcohol domain, the variation of $2R$ with excess alcohol (ϕ) can be written as:

$$2R(\phi) = 2R_0 + 2\Delta R(1 - e^{-\phi/\Phi}) \quad (1)$$

where $2R_0$ is the size corresponding to the stock solution, $2\Delta R$ is related to the change in size and Φ is related to the critical

Table 2 In-plane (b) and out-of-plane (c) unit cell parameters of the compressed 2D-hexagonal structure, the ratio of semi-major and semi-minor axis (r_l/r_s) corresponding to the equivalent ellipse and estimated as-prepared film thickness (D_0) for the different films on differently-terminated Si substrates. Subscripts i and f represent parameters corresponding to the initial and final time of measurements, respectively

Sample	b (nm)	c_i (nm)	c_f (nm)	$(r_l/r_s)_i$	$(r_l/r_s)_f$	D_0 (nm)
OH(0)	5.42	7.42	5.80	1.26	1.62	
H(0)	5.38	7.04	5.80	1.32	1.61	
OH(15)	5.23		6.12		1.48	80
H(15)	5.19		6.44		1.40	72
OH(20)	5.17		6.20		1.44	70
H(20)	5.19		6.40		1.40	68
OH(30)	5.16		6.32		1.41	52
H(30)	5.16		6.36		1.41	47
OH(35)	5.19	7.64	6.30	1.18	1.43	43
H(35)	5.19	7.28	6.82	1.24	1.32	39

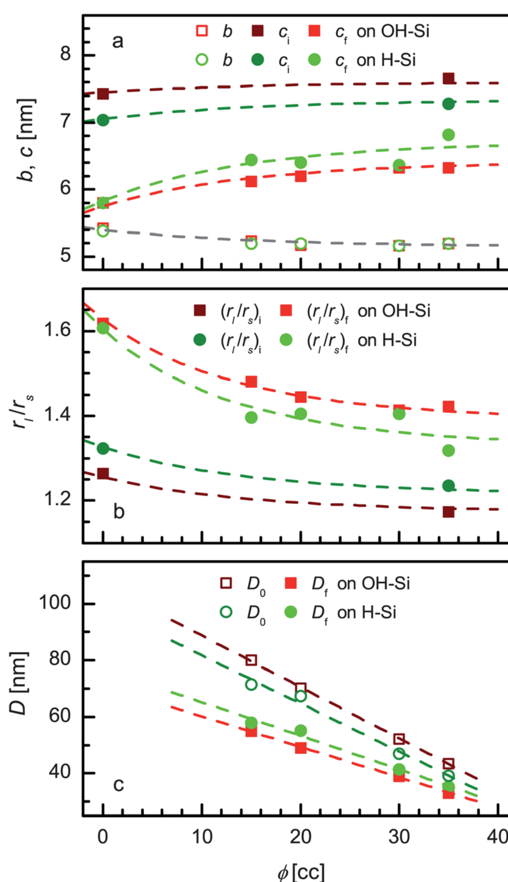

Fig. 8 Influence of excess alcohol (ϕ) on (a) the in-plane (b) and out-of-plane (c) unit cell parameters of the compressed 2D-hexagonal structure, (b) the ratio of semi-major and semi-minor axis (r_l/r_s) of corresponding ellipse and (c) the film thickness (D) for the different films on hydrophilic and hydrophobic Si substrates. Dashed lines through the data points in (a) and (b) are the analyzed curves and in (c) are the straight lines. Subscripts 0, i and f represent parameters corresponding to the as-prepared time and to the initial and final time of measurements, respectively.

amount of the excess alcohol. Second consider the in-plane separation (b), the value of which is a sum of the size of a micelle ($2R$) and the thickness of the silica wall. Due to the attachment of the film with the substrate, there should not be any in-plane movement of materials in the film with time (t), hence b should be independent of t. The variation or decrease of b with excess alcohol, as observed experimentally, can be expressed as:

$$b(\phi) = b_0 - \Delta b(1 - e^{-\phi/\Phi}) \quad (2)$$

where b_0 is the in-plane separation corresponding to the stock solution, Δb is the change in separation, which is related to the combined change in the size and in the silica wall thickness. Third consider the ratio r_l/r_s (or $2r_l/2r_s$). The in-plane size, $2r_l$ is nothing but b, which is a function of ϕ, but independent of both t and nature of the substrate, while the out-of-plane size, $2r_s$ depends on all three parameters (ϕ, t and nature of the substrate). The decrease of $2r_s$, initially on hydrophobic substrate, is due to the change in the shape of micelles from circular to elliptical, while with time, is essentially due to contraction of silica materials,

which also changes the shape of the micelles. The contraction of silica materials depends on the silica wall thickness and initial shape of micelles. Considering all these aspects, variation of r_l/r_s can be expressed as:

$$\begin{aligned}\frac{r_s}{r_l}(\phi,t) &= \frac{fb(\phi) - \Delta\left[b(\phi) - 2R(\phi)/f^2\right]\left(1 - e^{-t/\tau}\right)}{b(\phi)} \\ &= f - \Delta\left[1 - \frac{1}{f^2}\frac{2R(\phi)}{b(\phi)}\right]\left(1 - e^{-t/\tau}\right)\end{aligned} \quad (3)$$

where $f \leq 1$ is a substrate nature dependent term, which takes into account the different initial shape of the micelles in the film. For a circular shape, $f = 1$; while for an in-plane elongated elliptical shape, $f < 1$. The second term essentially takes into account the change with time, where Δ and τ are the critical decay constant and time, respectively. Such change is also related to the silica wall thickness and the initial shape of the micelles, which have been taken care of by the square bracket term. Note that for $t = 0$, $r_l/r_s = 1/f$ and for $f = 1$, $r_l/r_s = 1$.

Eqn (1 to 3) have been used to simulate the variation of b, c and r_l/r_s. For the simulation, a set of values for different parameters (other than that for f) is used for all the samples. First the variation of b has been fitted using eqn (2). The fitted profile is shown in Fig. 8 and the value of the parameters (Φ, b_0 and Δb) are listed in Table 3. Next, the variation of r_l/r_s and c [$= \sqrt{3}b/(r_l/r_s)$] have been simulated using eqn (1 to 3). For the simulation we have fixed the value of $2R_0 \approx 3$ nm, which we obtained by preparing a film containing micelles only (see supplementary information†). The analyzed profiles are shown in Fig. 8 and the parameters obtained from the analysis are listed in Table 3, which are useful to predict the evolution of the structure of the film, as discussed in the next section. Furthermore, the film thickness at the time of preparation (*i.e.* $t \approx 0$) can also be estimated considering $D_0 = f(d_{fs} + d_t + \sqrt{3}bN/2)$ and using $d_{fs} + d_t \approx 3$ nm (as obtained for the thin film) and the values of N, b and f, as listed in Tables 1 to 3. The value of D_0 thus obtained are listed in Table 2. Such a value of D_0 along with the value of D_f are plotted in Fig. 8(c), which show an almost linear decrease with excess alcohol. However, the value of D and its change with excess alcohol for the films on OH–Si are initially (*i.e.* $t \approx 0$) large, but finally become small compared to those for the films on H–Si.

3.3 Formation mechanism

The evolution of the structures on OH–Si and H–Si substrates are shown schematically in Fig. 9. Before elaboration of such model structures, let us first discuss the general formation mechanism of the silica–surfactant mesostructure. Above cmc, surfactants aggregate and form micelles. It is formed by a process of force balance in which no strong covalent bonding is involved.[11,20,43] The initial shape of such micelle is mostly spherical, which can be transformed to another shape depending upon the solution conditions. It is known that in the acid synthesis route, the mesostructured silica is formed by a weak electrostatic interaction between the cationic surfactant head group (S^+) and the positively charged silica oligomer (I^+), mediated by a counterion (X^-).[44,45] Hence the initial micelle formation is fast but the silica condensation is slow. The surfactants first adsorb the counterions to form the S^+X^- micelles, while in acidic solution, the hydrolysis and protonation of TEOS first generates the positively charged silica species as $\equiv SiOH_2^+$ (denoted as I^+). In the mixed solution, the condensation reaction of I^+ occurs on the counterion-adsorbed micelle surface ($S^+X^-I^+$) and once enough silica condensation has occured to form long polysilicate chains, then those chains act as bridges between micelles (having the hydrophobic tail part inside and the hydrophilic head group outside) to form the mesostructure. The final shape of micelles and their arrangement in the film, however, depend on the solution conditions. The concentration of CTAB, CTAB : TEOS ratio, pH and temperature *etc.* chosen for the present experiment are such that they lead to the formation of cylindrical micelles in a 2D-hexagonal structure.[2–4,7]

It is known that the OH–Si substrate is hydrophilic, while the H–Si substrate is hydrophobic in nature, which can be easily verified from the wetting or dewetting properties of the water with the surface by the naked eye, apart from contact angle measurements.[46] Such different nature of the substrates will exert different forces on the silica coated aggregates. Accordingly, the initial attachment of the film on the hydrophilic substrate is *via* silica coated cylindrical structured micelles, while that on the hydrophobic substrate is *via* hemicylindrical structured micelles. As the OH–Si surface is hydrophilic and anionic in nature, they can attract the positively charged silica coated micelles ($S^+X^-I^+$) by electrostatic interaction to lower the free energy of the system. As a result, a silica buffer layer is found on the Si substrates and above it there are cylindrical micelles (as shown schematically in Fig. 9). On the other hand, the H–Si substrate, due to its hydrophobic nature, can not form hydrogen bonds with water, rather it tries to cover-up with the surfactant hydrophobic tails to reduce the water exposer on it and also the free energy of the system. The best possible reduction for such a silica coated micellar system is however possible by formation of hemicylindrical micelles with reduced curvature on the substrate (as shown schematically in Fig. 9).

The cylindrical micelles are then stacked above the first micellar layer, the shape of which is strongly influenced by the curvature of the micelles in the first layer. For the as-prepared films, the near circular micelles on the OH–Si substrate with $r_l/r_s \approx 1$ become elliptical on the H–Si substrate with $r_l/r_s \approx 1.1$ (as shown schematically in Fig. 9 for $t \approx 0$ and $\phi = 0$). Next, when excess alcohol is added to the solution just before

Table 3 Different parameters used for the simulation of the size, shape and separation of the micelles in the films on the two differently-terminated Si substrates

Substrate	Φ (cm^3)	b_0 (nm)	Δb (nm)	$2R_0$ (nm)	$\Delta 2R$ (nm)	τ (h)	Δ	f
OH–Si	15	5.4	0.25	3.0	0.45	20	0.85	1.0
H–Si	15	5.4	0.25	3.0	0.45	20	0.85	0.9

 This journal is © The Royal Society of Chemistry 2012

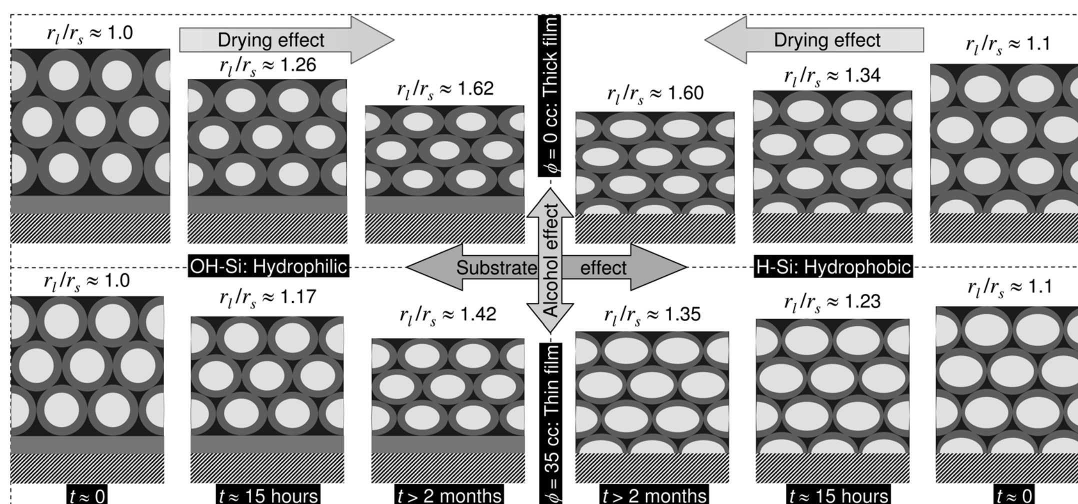

Fig. 9 Model cross-sectional views of the CTAB–silica mesostructures just after deposition ($t \approx 0$) and in the initial ($t \approx 15$ h) and final ($t > 2$ months) stages of measurements for the thick ($\phi = 0$) and thin ($\phi = 35$ cm^3) films on OH–Si and H–Si substrates as predicted from XR and GISAXS results, showing the effects of substrate, alcohol and time (drying) on the r_l/r_s value, on the attachment of the films on the substrates, and on the size, separation and shape of the micelles in the films.

deposition, it acts as both cosolvent and cosurfactant. As a cosolvent it dilutes the solution, which decreases the repetition number and the silica coating layer thickness, while as cosurfactant it resides on the outer boundaries of the micelles, which increases the effective head group area of the surfactant molecule[30] and hence the size of the micelles (from ~3.0 to 3.45 nm, obtained from $2R_0$ and $2\Delta R$ values). Combination of the coating layer thickness and the micelles size, decreases the overall separation, which showed up in the value of b (from ~5.40 to 5.15 nm, obtained from b_0 and Δb_0 values) only, but not in r_l/r_s (as shown schematically in Fig. 9 for $t \approx 0$ and $\phi = 35$ cm^3). Further, with the addition of excess alcohol the silica coating thickness decreases from ~2.4 to 1.7 nm, which is shown up on the hydrophilic substrate. On the hydrophobic substrate, the micelles become elongated (with size $2R/f^2$) along the in-plane direction. So, on such a substrate, the in-plane size of the micelles changes from ~3.7 to 4.25 nm with addition of excess alcohol and the corresponding in-plane silica wall thickness changes from ~1.7 to 0.9 nm.

The structures of the films, that we discussed so far, are formed just after deposition, that is due to the fast evaporation of solvent while spin coating. Such structures further modified with time, as presented in Fig. 9 for the initial and final stages of measurements and can be visualized as follows. With time, the thickness of the coated silica layer decreases due to the drying effect. Such a decrease is only allowed in the out-of-plane direction but not in the in-plane direction (due to the attachment of the film with the substrate). This also decreases the size of the micelles and the separation between them along the out-of-plane direction, which in turn changes the shape of the micelles by squeezing them along the out-of-plane direction and the value of r_l/r_s, respectively. It is necessary to mention that the value of the silica coated layer thickness (b–$2R$), which seems to be quite large (~2.4 to 1.7 nm) initially becomes quite reasonable (~1.5 to 1.2 nm) with time due to drying, as obtained from out-of-plane information. The change in the r_l/r_s value seems to depend on the initial in-plane silica wall thickness. If such thickness is large (which is for the films prepared with $\phi = 0$) then the change is large, while if thickness is small (which is for the films prepared with $\phi = 35$ cm^3) then the change is also small. Considering the different initial shape of the micelles on the OH–Si and H–Si substrates, the largest initial silica wall thickness (~2.4 nm) is estimated for the thick film on the OH–Si substrate and the corresponding change in the value of r_l/r_s is at its maximum (~0.62; change from 1 to 1.62), while smallest in-plane silica wall thickness (~0.9 nm) is estimated for the thin film on the H–Si substrate and the corresponding change in the value of r_l/r_s is at its minimum (~0.25; change from 1.1 to 1.35). However, in terms of the shape of the micelles, the maximum and minimum deviations from the circular shape are observed for the thick film on the H–Si substrate and the thin film on the OH–Si substrate, respectively. Also with time, due to the asymmetric shrinkage of the silica wall and hence also of the micelles, the stress is developed in the film, which deteriorates the ordering in the film. For the thick film, both the number of repetitive micelles layers (N) and the silica wall thickness are big, hence the stress is large.

4. Conclusions

Structural evolution of evaporation-induced self-assembled CTAB–silica mesostructured films on differently-treated Si substrates were monitored using XR and GISAXS techniques. A centered rectangular (*c*2*mm* space group) structure is observed in dried films on both the substrates showing clear deviation from the perfect 2D-hexagonal (*p*6*m*) structure. Such deviation is directly related to the change in shape of the micelles in the film. With time the silica materials try to squeeze due to drying, which can be expressed exponentially with critical drying time of ~1 day. However, squeezing is not allowed along the in-plane direction due to the attachment of the film on the substrate. Such asymmetric squeezing compressed the structure and also developed stress. The latter deteriorates the ordering of the film. The

compression depends on the silica wall thickness; the more thickness, the more compression. The silica wall thickness again depends on the amount of excess alcohol. The more excess alcohol we added, the less the film and silica coating layer thickness becomes, hence the compression and stress, which are clearly observed in the structure of the film. Excess alcohol not only acts as a cosolvent as mentioned before, but also act as a cosurfactant. According to the latter, the size of the micelles increases exponentially with a critical amount of excess alcohol of ~15 cm^3. Analysis of the XR data measured at different time intervals and the GISAXS data measured for the dried film suggest that during deposition, cylindrical shaped micelles are circular on OH–Si and form a perfect 2D-hexagonal structure (with $r_l/r_s \approx 1$), while elliptical on H–Si and form a compressed 2D-hexagonal structure (with $r_l/r_s \approx 1.1$). Such difference in shape is related to different attachment of the film with the substrate, namely silica on the hydrophilic OH–Si substrate and hemicylindrical micelles on the hydrophobic H–Si substrate. For the dried films, the maximum and minimum deformed structures (*i.e.* $r_l/r_s \approx 1.62$ and 1.35) are observed for the thick film on OH–Si and for the thin film on H–Si, respectively. However, considering the shape of the micelles, the maximum and minimum deformed shapes are predicted for the thick film on H–Si and for the thin film on OH–Si, respectively. Combining the initial shape and the effect of compression with time, which are related to the nature of the substrate and the amount of excess alcohol, respectively, the final structures of the dried films along with the shape of the micelles are formed, which are of immense importance for their proper use as templates and other applications.

Acknowledgements

Financial support received under Indo-Italian POC to carry out GISAXS experiments at Elettra is thankfully acknowledged.

References

1 J. S. Beck, J. C. Vartuli, W. J. Roth, C. T. K. M. E. Leonowicz, K. D. Schmitt, C. T. W. Chu, D. H. Olson and E. W. Sheppard, *J. Am. Chem. Soc.*, 1992, **114**, 10834.
2 C. J. Brinker, Y. Lu and A. Sellinger, *Adv. Mater.*, 1999, **11**, 579.
3 S. Besson, T. Gacoin, C. Ricolleau, C. Jacquiod and J.-P. Boilot, *J. Mater. Chem.*, 2003, **13**, 404.
4 L. Nicole, C. Boissiere, D. Grosso, A. Quach and C. Sanchez, *J. Mater. Chem.*, 2005, **15**, 3598.
5 M. Matheron, A. Bourgeois, A. Brunet-Bruneau, P. A. Albouy, J. Biteau, T. Gacoin and J.-P. Boilot, *J. Mater. Chem.*, 2005, **15**, 4741.
6 Y. Lu, R. Ganguli, C. A. Drewien, M. T. Anderson, C. J. Brinker, W. Gong, Y. Guo, H. Soyez, B. Dunn, M. H. Huang and J. I. Zink, *Nature*, 1997, **389**, 364.
7 D. A. Doshi, A. Gibaud, V. Goletto, M. Lu, H. Gerung, B. Ocko, S. M. Han and C. J. Brinker, *J. Am. Chem. Soc.*, 2003, **125**, 11646.
8 A. Gibaud, D. Grosso, B. Smarsly, A. Baptiste, J. F. Bardeau, F. Babonneau, D. A. Doshi, Z. Chen, C. J. Brinker and C. Sanchez, *J. Phys. Chem. B*, 2003, **107**, 6114.
9 D. A. Doshi, A. Gibaud, N. Liu, D. Sturmayr, A. P. Malanoski, D. R. Dunphy, H. Chen, S. Narayanan, A. MacPhee, J. Wang, S. T. Reed, A. J. Hurd, F. Swol and C. J. Brinker, *J. Phys. Chem. B*, 2003, **107**, 7683.
10 Q. Huo, D. I. Margolese and G. D. Stucky, *Chem. Mater.*, 1996, **8**, 1147.
11 Y. S. Lee, *Self-assembly and nanotechnology: a force balance approach*, John Wiley, NJ, USA, 2008.
12 F. Cagnol, D. Grosso, G. J. A. A. Soler-Illia, E. L. Crepaldi, F. Babonneau, H. Amenitsch and C. Sanchez, *J. Mater. Chem.*, 2003, **13**, 61.
13 A. Gibaud, S. Dourdain, O. Gang and B. M. Ocko, *Phys. Rev. B: Condens. Matter Mater. Phys.*, 2004, **70**, 161403(R).
14 M. Matheron, T. Gacoin and J.-P. Boilot, *Soft Matter*, 2007, **3**, 223.
15 S. Manne, J. P. Cleveland, H. E. Gaub, G. D. Stucky and P. K. Hansma, *Langmuir*, 1994, **10**, 4409.
16 S. Manne and H. E. Gaub, *Science*, 1995, **270**, 1480.
17 L. M. Grant and W. A. Ducker, *J. Phys. Chem. B*, 1997, **101**, 5337.
18 L. M. Grant, F. Tiberg and W. A. Ducker, *J. Phys. Chem. B*, 1998, **102**, 4288.
19 J. F. Liu and W. A. Ducker, *J. Phys. Chem. B*, 1999, **103**, 8558.
20 M. J. Rosen, *Surfactants and interfacial phenomena*, John Wiley, NJ, USA, 2004.
21 A. Imanishi, M. Suzuki and Y. Nakato, *Langmuir*, 2007, **23**, 12966.
22 H. F. Okorn-Schmidt, *IBM J. Res. Dev.*, 1999, **43**, 351.
23 X. G. Zhang, *Electrochemistry of silicon and its oxide*, Kluwer Academic, New York, 2004.
24 C. Y. Ruan, V. A. Lobastov, F. Vigliotti, S. Chen and A. H. Zewail, *Science*, 2004, **304**, 80.
25 J. K. Bal and S. Hazra, *Phys. Rev. B: Condens. Matter Mater. Phys.*, 2007, **75**, 205411.
26 J. K. Bal and S. Hazra, *Phys. Rev. B: Condens. Matter Mater. Phys.*, 2009, **79**, 155412.
27 P. L. Silvestrelli, F. Toigo and F. Ancilotto, *J. Phys. Chem. C*, 2009, **113**, 17124.
28 J. K. Bal, S. Kundu and S. Hazra, *Phys. Rev. B: Condens. Matter Mater. Phys.*, 2010, **81**, 045404.
29 H. Yang, N. Coombs, I. Sookolv and G. A. Ozin, *J. Mater. Chem.*, 1997, **7**, 1285.
30 S. Liu, P. Cool, O. Collart, P. V. D. Voort, E. F. Vansant, O. I. Lebedev, G. V. Tendeloo and M. Jiang, *J. Phys. Chem. B*, 2003, **107**, 10405.
31 I. K. Robinson and D. J. Tweet, *Rep. Prog. Phys.*, 1992, **55**, 599.
32 *X-Ray and neutron reflectivity: principles and applications*, ed. J. Daillant and A. Gibaud, Springer, Paris, 1999.
33 A. Naudon and D. Babonneau, *Z. Metallkd.*, 1997, **88**, 596.
34 S. Hazra, A. Gibaud, A. Desert, C. Sella and A. Naudon, *Phys. B*, 2000, **283**, 97.
35 A. Gibaud, A. Baptiste, D. A. Doshi, C. J. Brinker, L. Yang and B. Ocko, *Europhys. Lett.*, 2003, **63**, 833.
36 S. Hazra, A. Gibaud and C. Sella, *Appl. Phys. Lett.*, 2004, **85**, 395.
37 A. J. Allen, *J. Am. Ceram. Soc.*, 2005, **88**, 1367.
38 S. Hazra, A. Gibaud and C. Sella, *J. Appl. Phys.*, 2007, **101**, 113532.
39 S. Hazra, *Appl. Surf. Sci.*, 2006, **253**, 2154.
40 H. Amenitsch, M. Rappolt, M. Kriechbaum, H. Mio, P. Laggner and S. Bernstoff, *Rev. Sci. Instrum.*, 1998, **5**, 506.
41 L. G. Parratt, *Phys. Rev.*, 1954, **95**, 359.
42 M. Klotz, P.-A. Albouy, A. Ayral, C. Menager, D. Grosso, A. V. der Lee, V. Cabuil, F. Babonneau and C. Guizard, *Chem. Mater.*, 2000, **12**, 1721.
43 J. Z. Zhang, Z. l. Wang, J. Liu, S. Chen and G. yu Liu, *Self-assembled nanostructures*, Kluwer Academic, New York, 2004.
44 Q. Huo, D. I. Margolese, U. Ciesla, D. G. Demuth, P. Feng, T. E. Gier, P. Sieger, A. Firouzi, B. F. Chmelka, F. Schuth and G. D. Stucky, *Chem. Mater.*, 1994, **6**, 1176.
45 H.-P. Lin, C.-P. Kao, C.-Y. Mou and S.-B. Liu, *J. Phys. Chem. B*, 2000, **104**, 7885.
46 J. K. Bal, S. Kundu and S. Hazra, *Chem. Phys. Lett.*, 2010, **500**, 90.

 This journal is © The Royal Society of Chemistry 2012